Earth and Planetary Science Letters 280 (2009) 236–245

Contents lists available at ScienceDirect

Earth and Planetary Science Letters

journal homepage: www.elsevier.com/locate/epsl

CRE dating on the head scarp of a major landslide (Séchilienne, French Alps), age constraints on Holocene kinematics

Olivier Le Roux [a], Stéphane Schwartz [a,*], Jean François Gamond [a], Denis Jongmans [a], Didier Bourles [b], Régis Braucher [b], William Mahaney [c], Julien Carcaillet [d], Laetitia Leanni [b]

[a] Laboratoire de Géophysique Interne et Tectonophysique (CNRS, UMR 5559), Observatoire des Sciences de l'Univers, Université Joseph Fourier, BP 53, F-38041, Grenoble cedex 09, France
[b] Centre Européen de Recherche et d'Enseignement des Géosciences de l'Environnement (CNRS, UMR 6635), Université Aix-Marseille, BP 80, F-13545 Aix en Provence cedex 04, France
[c] Geomorphology and Pedology Lab, York University, 4700 Keele St.,N. York, Ontario, Canada M3J 1P3
[d] Laboratoire de Géodynamique des Chaînes Alpines (CNRS, UMR 5025), Observatoire des Sciences de l'Univers, Université Joseph Fourier, BP 53, F-38041, Grenoble cedex 09, France

ARTICLE INFO

Article history:
Received 9 October 2008
Received in revised form 23 January 2009
Accepted 24 January 2009
Available online 14 February 2009

Editor: T.M. Harrison

Keywords:
cosmic ray exposure method
Séchilienne landslide kinematics
head scarp dating
Holocene climatic optimum

ABSTRACT

Cosmic Ray Exposure (CRE) dating applied to the active Séchilienne landslide (Romanche valley, Belledonne Massif, French Alps) provides information about its Holocene dynamics from initiation to present day activity. Glacier retreat at 1100 m a.s.l. is estimated at 16.6 ± 0.6 ^{10}Be ka from glacially polished bedrock samples, with total deglaciation of the valley achieved at least by 13.3 ka. Application of the CRE method along vertical profiles sampled with a high spatial resolution of 3 m on the head scarp yields: (1) an initiation of the rock-slope failure at 6.4 ± 1.4 ^{10}Be ka and (2) a continuous rock-slope failure activity with a mean head scarp exposure rate of 0.6 cm/yr. The data suggest an increase of the head scarp exposure rate between 2.3 and 1.0 ka. After this acceleration phase, the exposure rate is similar to that obtained by the present day monitoring data over 20 years in the depletion zone (1.3 cm/yr). Since the failure initiation occurred more than 5400 yr after the total deglaciation of the valley the slope failure does not appear as an immediate consequence of debutressing in the Romanche valley. This result is consistent with studies of other large alpine rockslides in the Alps. Failure initiation of the Séchilienne landslide occurred during the Holocene Climatic Optimum, a hot and wet period. The temperature and precipitation changes of this climatic optimum seem to have a worsening effect at the regional scale to trigger large mass wasting in this glacial alpine valley.

1. Introduction

One of the most significant geomorphological consequences of deglaciation in mountainous valleys is the exposure of steepened rock slopes which have been identified as gravitationally unstable areas (Augustinus, 1995; Erismann and Abele, 2001; Ballantyne, 2002). Lateral stress release resulting from ice melting (debutressing) has been frequently recognized as a major cause triggering rock-slope failure in deglaciated mountain areas (among others, Gardner, 1980; Cruden and Hu, 1993; Blair, 1994; Evans and Clague, 1994; Holm et al., 2004; Cossart et al., 2008). However, other factors like tectonic stresses, uplift rate, river and bedrock erosion, earthquakes and subsequent climatic changes have also been evoked, as contributing to large rock-slope instabilities (Ballantyne and Stone, 2004; Seijmonsbergen et al., 2005; Cossart et al., 2008; Hormes et al., 2008; Korup et al., 2008). Identifying the cause responsible for triggering large slope failures in mountain ranges, where all the above mentioned factors are potentially active, is a delicate task and remains a debated question (Korup et al., 2007). The main approach applied so far for evaluating a link between deglaciation and rock-slope instability has been to study the timing of specific landslides, using ^{14}C dating and Cosmic Ray Exposure (CRE) dating. Even if radiocarbon ages provide valuable information on the chronology of major landslides like the Flims rockslide (Eastern Switzerland; Deplazes et al., 2007) and the Fernpass rockslide (Austria, Prager et al., 2009), the ^{14}C method is, however, limited by the difficulty of finding in situ organic matter coeval with landslide events. On the contrary, surface exposure dating using cosmogenic nuclides such as ^{10}Be and ^{36}Cl appear to be widely applicable for quartz-bearing and calcareous rocks (Gosse and Phillips, 2001) exposed to the subaerial atmosphere. Samples for dating landslides can be collected from bedrock scarps (Bigot-Cormier et al., 2005; Hippolyte et al., 2006; Ivy-Ochs et al., 2009; Prager et al., 2009) and/or from rock avalanche deposits (Ballantyne and Stone, 2004; Cossart et al., 2008; Hormes et al., 2008; Ivy-Ochs et al., 2009; Prager et al., 2009). One major advantage of CRE dating methods is that they are also able to constrain the timing of the last deglaciation by dating late glacial moraine deposits and glacially polished bedrock surfaces (Gosse et al., 1995; Owen et al., 2001; Carlson et al., 2007; Delmas et al., 2008). Several studies recently focused on the chronology of valley deglaciation and rock-slope instability at specific sites (Bigot-Cormier et al., 2005;

* Corresponding author.
E-mail address: stephane.schwartz@ujf-grenoble.fr (S. Schwartz).

0012-821X/$ – see front matter © 2009 Elsevier B.V. All rights reserved.
doi:10.1016/j.epsl.2009.01.034

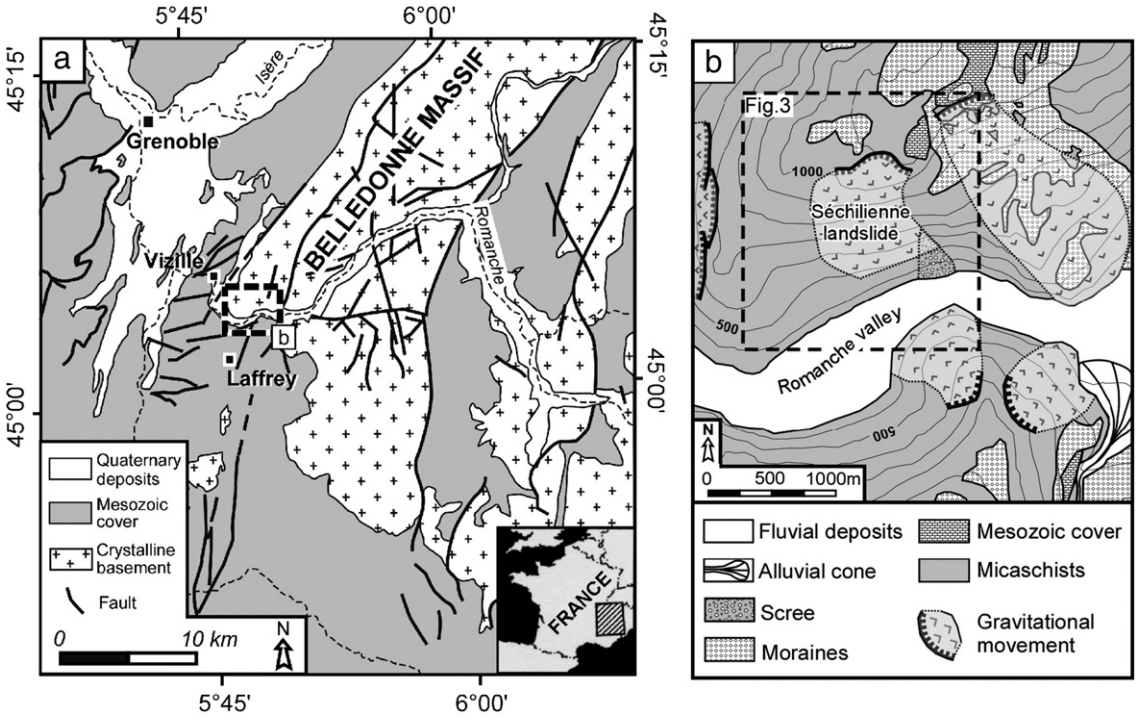

Fig. 1. (a) Structural map of the southwestern part of the Belledonne External Crystalline Massif centred on the lower Romanche Valley. The polygon in dashed line locates Fig. 1 b. (b) Geological and geomorphological map of the lower Romanche Valley. The polygon in dashed line locates Fig. 2.

Cossart et al., 2008; Hormes et al., 2008; Ivy-Ochs et al., 2009; Prager et al., 2009). Surface exposure ages tend to indicate that the largest landslides in the Alps did not occur during deglaciation but in mid-Holocene time when climate became warmer and wetter. The Fernpass (Austria, 4100 yr), Flims (Switzerland, 8900 yr), Kandertal (Switzerland, 9600 yr), Köfels (Austria, 9800 yr), La Clapière (France, 10,300 yr), Valtellina (Italy, 7430 yr) landslides occurred at least a few thousand years after deglaciation. The Séchilienne landslide, which affects the south-facing crystalline slope of the glaciated Romanche Valley, is one of the largest in the French Alps. Based on CRE dating, this study first aims

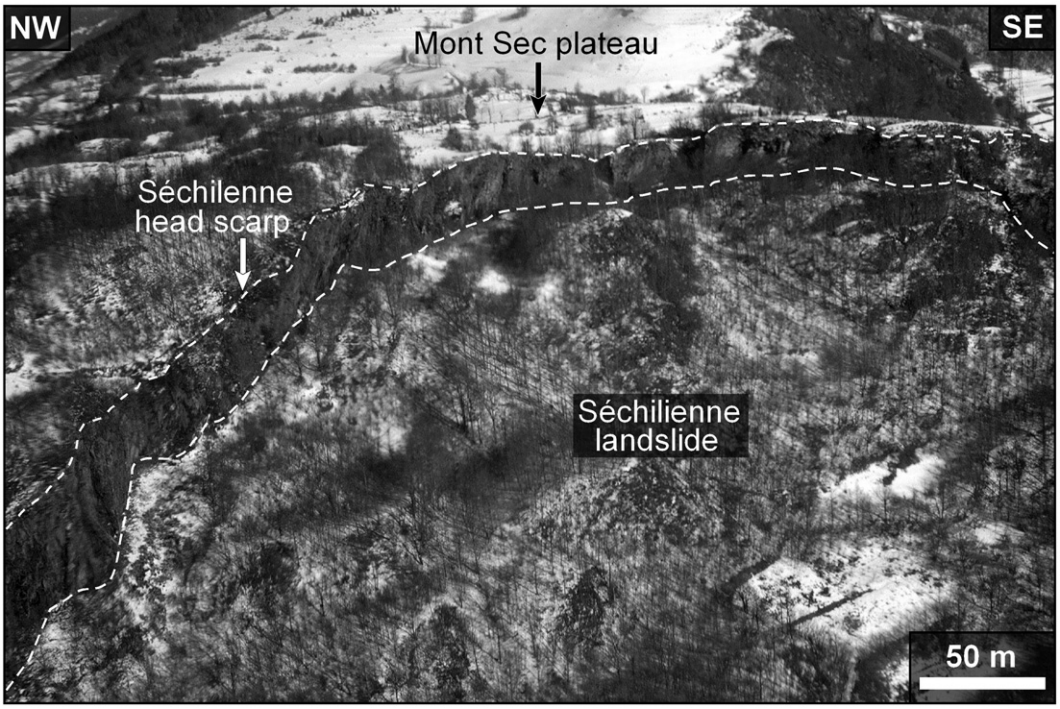

Fig. 2. Aerial photograph of the Séchilienne landslide (provided by M. Gidon, www.geol-alp.com) between 1000 m and the Mont Sec plateau at 1100 m a.s.l. The head scarp is outlined by white dotted lines. It constitutes the upper limit of the unstable area.

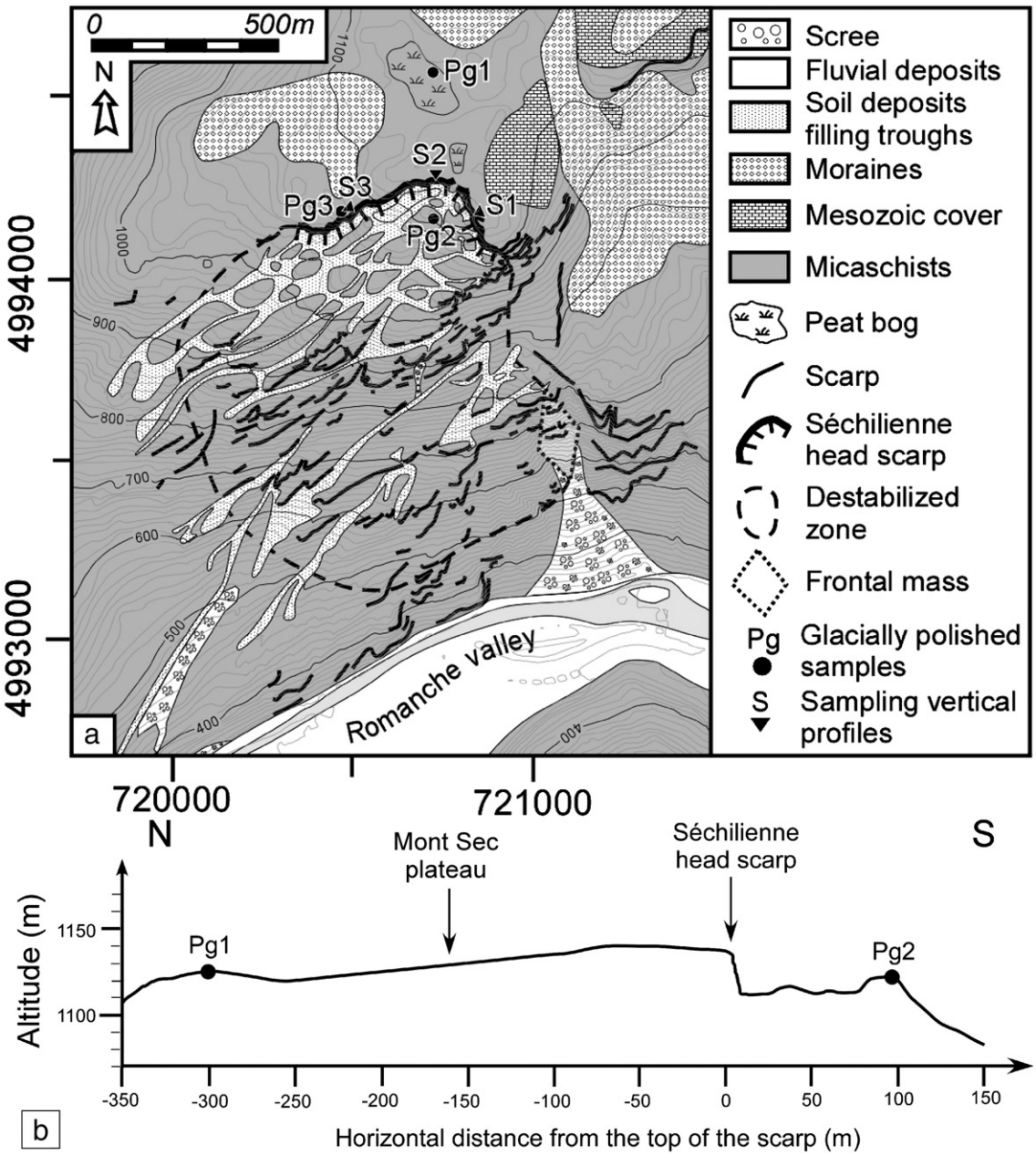

Fig. 3. (a) Geological and geomorphological detailed map of the Séchilienne landslide with the location of sampling sites. (b) North-South cross section between Pg1 and Pg2 show the Séchilienne head scarp at the upper boundary of the destabilized zone, scale 1/1.

to determine the age of release of bedrock and emplacement and to compare it to timing of deglaciation. The paper is also focused on placing temporal constraints on the Séchilienne motion (kinematics) by regularly sampling the head scarp surface along vertical profiles. Exposure ages suggest a change in the kinematics of the landslide during the late Holocene.

2. Structure and dynamics of the landslide

The Séchilienne landslide is located in the southwestern part of the Belledonne Massif (western Alps) (Fig. 1). The massif extends over more than 120 km in a N30 direction, is almost 3000 m high, and is bounded to the west by the large topographic depression of the Isère Valley (Fig. 1a). The massif, one of the Palaeozoic External Crystalline Massifs of the French Alps, is part of the Hercynian orogen reworked during the Alpine orogenesis. These basement rocks consist of a complex of different metamorphic rocks (gneisses, amphibolites and micaschists). The study area to the west of the massif features mainly micaschists unconformably covered with Mesozoic sediments and Quaternary deposits (Fig. 1b). In the southern part of the Belledonne Massif these micaschists are dissected by the East–West trending lower Romanche River (Fig. 1). Incision of these rocks results from the alternate activity of water and ice in the Romanche River during a succession of Quaternary glaciations (Montjuvent and Winistorfer, 1980). The resulting morphology displays steep slopes, around 35 to 40°, affected by active or paleo large-scale rock mass deformation between 400 and 1100 m elevation (Barféty et al., 1970; Le Roux et al., 2008) (Figs. 1b and 2). Above 1100 m, the morphology corresponds to a glacial plateau where moraine deposits and peat bogs subsist (Figs. 2 and 3b).

Among these unstable slopes, the Séchilienne landslide, located on the right bank of the Romanche River (Figs. 1b and 3a), is the most active one. The upper boundary of the movement is several hundred meters wide with several tens of meters high vertical head scarp

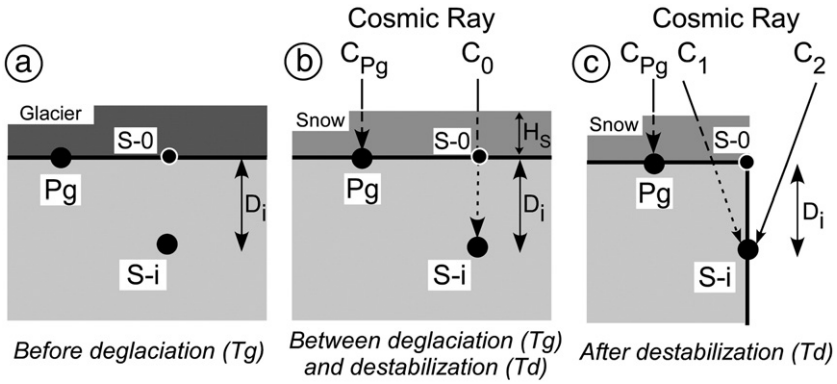

Fig. 4. Model used for the computation of the exposure ages with the Pg2 age taken as the reference age of the deglaciation (a) $T<Tg$. (b) $Tg<T<Td$. (c) $Td<T<0$. Pg: glacially polished bedrock sample. S-i: location of the sample on the vertical scarp. Di: distance between the upper edge of the scarp and S-i. Tg: age of the retreat of the glacier. Td: age of the destabilization.

(Séchilienne head scarp, see Fig. 2, Fig. 3). This scarp separates the flat stable glacial Mont Sec Plateau from the destabilized zone. The metamorphic rocks within the landslide are cut by two sets of near-vertical fractures with directions N60 and N140, respectively, with unknown vertical depth. This structural framework results in linear scarps and troughs filled by rocks debris and topsoil (Fig. 3a), which delineate rock blocks displaying down slope motion. Below the head scarp, the low-slope depletion zone between 1100 and 950 m a.s.l. exhibits a series of large depressions and salient blocks (Fig. 3). The lower part of the landslide, between 950 and 450 m a.s.l., shows steep convex slopes (>40°, Fig. 3a) interpreted as an accumulation zone (Vengeon, 1998). In 1993–1994, a 240 m long gallery was excavated at 710 m revealing a succession of rigid moving blocks delimited by highly fractured zones (Vengeon, 1998). This gallery did not reach the sound rock and the existence of a sliding surface is still an open question. Hydrochemical investigation (Vengeon, 1998; Guglielmi et al., 2002) suggested the existence of a deep phreatic zone extending into the fractured metamorphic bedrock, with a probable 100 m thick vadose zone above. With intensive rainfall and long-term water recharge (>45 days), this vadose zone could be saturated during rainy periods, increasing the displacement rate (Vengeon, 1998).

Since the 1980's, a monitoring system (extensometers, geodetic measurements, tacheometers and microwave radar) has progressively been installed by the *Centre d'Etudes Techniques de l'Equipement* (CETE) of Lyon (Evrard et al., 1990; Vengeon et al., 1999; Duranthon et al., 2003). Monitoring results show: (1) homogeneous orientations (N140) and inclinations (10 to 20°) of displacement vectors over the whole sliding mass; and (2) a partition of the landslide into two zones with different slide velocity vectors. The global destabilized mass, with a volume of more than 25×10^6 m^3, displays medium activity with slow displacement rates (2 to 15 cm/yr) (Giraud et al., 1990; Durville et al., 2004). In this zone the vertical displacement component at the base of the head scarp yields a subsidence rate between 0.7 and 1.6 cm/yr with a mean value of 1.3 cm/yr (Vengeon et al., 1999). Lower in the slope, a frontal mass with a volume of about 3×10^6 m^3 exhibits high sliding velocity vectors reaching a maximum of 100 cm/yr. This frontal movement generates frequent rock falls. The displacement rate series in this zone exhibits seasonal variations, with an increase by a factor of three during heavy rainfall and snow melting periods in winter and spring (Rochet et al., 1994; Alfonsi, 1997; Vengeon, 1998; Durville et al., 2004). The mechanism usually proposed for the Séchilienne landslide activity is slope unloading and consecutive stress release (debuttressing) following ice melting during the late Würmian retreat stage of the Romanche Glacier (15,000 yr BP) (Vengeon et al., 1999, Pothérat and Alfonsi, 2001). At the present time, monitoring data show that the kinematic behaviour of the landslide is hydraulically controlled by heavy rainfall and snow melt in winter and spring. Recently, Meric et al. (2005) performed a geophysical test on the Séchilienne landslide, which showed that the moving zone is identified by higher resistivity and lower P-wave velocity, compared to the stable area. They interpreted these results as the consequence of a higher fracturing degree in the micaschists.

3. Sampling strategy and methodology

Cosmic Ray Exposure dating is based on the accumulation of rare nuclides produced through nuclear reactions induced by high-energy cosmic radiation when rock is exposed at the earth's surface (Siame et al., 2000; Gosse and Philips, 2001). In this study we used *in situ* produced ^{10}Be resulting from spallation reactions on Si and O in quartz. Quartz was isolated and purified from samples and targets prepared for Accelerator Mass Spectrometer (AMS) analyses of ^{10}Be (Brown et al., 1991, 1998). All samples are crushed and sieved prior to initiating chemical procedures. The extraction method for ^{10}Be consists of isolation and purification of quartz and elimination of atmospheric ^{10}Be. Accurately 100 µl of a 3.10^{-3} g/g ^{9}Be solution is added to decontaminated quartz. Beryllium was separated from the spiked solution obtained after its dissolution in HF by successive solvent extraction and precipitation. The final precipitate is dried and heated at 900 °C to obtain BeO from which targets for measurements of the ^{10}Be concentration into our samples (N) are prepared. Measurements were performed at the new French AMS National Facility, ASTER, located at CEREGE in Aix-en-Provence. The data were calibrated directly against the National Institute of Standards and Technology (NIST) standard reference material 4325 by using the values recently determined by Nishiizumi et al. (2007), which are a ^{10}Be/^{9}Be ratio of $2.79\pm0.03\ 10^{-11}$ and a ^{10}Be half-life ($T_{1/2}$) of $1.36\pm0.07\ 10^6$ years, i.e. a radioactive decay (λ) of $5.10\pm0.26\ 10^{-7}$.

A modern ^{10}Be production rate at sea-level and high-latitude of 4.5 ± 0.3 atoms/g/yr, computed for internal consistency, from the data of Stone (2000), according to the conclusions of the study on absolute calibration of ^{10}Be AMS standards by Nishiizumi et al. (2007), was used. This sea-level and high-latitude production rate has then been scaled for the sampling altitudes and latitudes using the scaling factors proposed by Stone (2000) because, using the atmospheric pressure as a function of altitude, he takes into account the physical properties of cosmic ray particle propagation in the atmosphere and includes an improved account for the muonic component in the total cosmogenic production. The obtained surface production rates (P_0) were then corrected for local slope and

Table 1
Cosmogenic ^{10}Be analytical data.

Sample		Location X (m)	WGS84 Y (m)	UTM 31N Z (m)	Di (m)	P_0 (atoms/g/yr)	St	Ss	P (atoms/g/yr)	N_{10} (atoms/g)	σN_{10} (atoms/g)	C_0/N_{10} (%)	C_1/N_{10} (%)	C_2/N_{10} (%)	T_{min} (yr)	σT_{min} (yr)
Glacial surface																
Site 1																
	Pql-I	720,720	4,994,560	1120.0		11.43	1.00	0.90	10.31	77,437	5812				7526	565
	Pgl-2	720,720	4,994,570	1120.0		11.43	1.00	0.90	10.31	126,746	4534				12,334	441
Site 2																
	Pg2	720,725	4,994,175	1121.0		11.44	0.98	0.95	10.67	176,621	6140				16,628	578
Site 3																
	Pg3	720,490	4,994,160	1080.0		11.08	0.93	0.90	9.32	139,574	4028				15,059	435
Scarps																
Profile SI	S1-0	720,830	4,994,190	1142.0	0.0	11.63	1.00	0.90	10.49							
	SI-I	720,830	4,994,190	1139.0	3.0	11.61	0.50	1.00	5.80	30408	1804	8.2	1.7	90.1	4727	280
	S1-2	720,830	4,994,190	1137.0	5.0	11.59	0.50	1.00	5.79	33,962	4699	3.8	1.0	95.2	5589	773
	S1-3	720,830	4,994,190	1131.8	10.2	11.54	0.50	1.00	5.77	20,542	1794	4.4	0.6	95.0	3387	296
	SI-4	720,830	4,994,190	1125.0	17.0	11.48	0.50	1.00	5.74	11,061	901	5.0	0.3	94.6	1825	149
	S1-5	720,830	4,994,190	1124.0	18.0	11.47	0.50	1.00	5.73	7740	1103	6.9	0.3	92.8	1252	178
	S1-6	720,830	4,994,190	1123.6	18.4	11.47	0.50	1.00	5.73	10,392	1581	4.9	0.3	94.8	1720	262
	S1-7	720,830	4,994,190	1121.0	21.0	11.44	0.50	1.00	5.72	11,695	1236	3.6	0.3	96.2	1969	208
	S1-8	720,830	4,994,190	1119.3	22.7	11.43	0.50	1.00	5.69	6982	2023	5.6	0.2	94.1	1155	335
	SI-9	720,830	4,994,190	1116.0	26.0	11.40	0.49	1.00	5.60	5982	864	5.5	0.2	94.4	1008	146
	SI-l0	720,830	4,994,190	1112.3	29.7	11.36	0.48	1.00	5.42	3370	970	8.1	0.2	91.8	571	164
	S1-11	720,830	4,994,190	1109.0	33.0	11.33	0.47	1.00	5.34	1730	722	13.5	0.1	86.4	280	117
Profile S2	S2-0	720,730	4,994,255	1,130.0	0.0	11.52	1.00	0.90	10.38							
	S2-I	720,730	4,994,255	1128.0	2.0	11.51	0.45	1.00	5.19	15,444	1718	49.8	2.5	47.8	1423	158
	S2-2	720,730	4,994,255	1126.5	3.5	11.49	0.45	1.00	5.18	6915	1271	37.6	1.0	61.4	819	151
	S2-3	720,730	4,994,255	1125.5	4.5	11.48	0.45	1.00	5.18	7576	2628	26.0	0.9	73.1	1070	371
	S2-4	720,730	4,994,255	1120.0	10.0	11.43	0.55	1.00	6.25	17,978	2196	5.2	0.5	94.3	2712	331
Profile S3	S3-0	720,495	4,994,160	1078.0	0.0	11.06	0.99	0.90	9.89							
	S3-I	720,495	4994,160	1071.0	7.0	11.00	0.55	1.00	6.08	29,833	3334	2.8	0.6	96.6	4742	530
	S3-2	720,495	4994,160	1066.5	15.0	10.96	0.50	1.00	5.47	6127	1509	12.0	0.4	87.6	982	242
	S3-3	720,495	4994,160	1062.5	17.5	10.92	0.50	1.00	5.45	9194	2534	5.6	0.3	94.1	1589	438
	S3-4	720,495	4994,160	1057.5	23.0	10.88	0.50	1.00	5.41	10,617	1931	3.4	0.2	96.4	1892	344

X: latitude. Y: longitude. Z: altitude. Di: distance between the upper edge of the scarp and the sample. P_0: production rate. St: topographic shielding factor. Ss: snow shielding factor. P: normalized production rate. N_{10}: concentration of ^{10}Be in the sample. σN_{10}: analytical standard deviation on N_{10}. C_0: concentration of ^{10}Be in the sample accumulated between Tg and Td at depth Di from the horizontal surface. C_1: concentration of ^{10}Be in the sample accumulated between Td and today at depth Di from the half of the horizontal surface. C_2: concentration of ^{10}Be in the sample accumulated between Td and today at the surface of the cliff.

topographic shielding due to surrounding morphologies (S_t), following Dunne et al. (1999), and for the presence of snow (S_s) to yield the sampling location production rates (P):

$$P = P_0 S_t S_s \tag{1}$$

We divided the samples into two series. In the first series, samples collected from glacially polished bedrock surfaces allowed determination of the approximate timing of the last deglaciation on top of the Séchilienne landslide (Pg1 to Pg3) (Fig. 3a). In the second series, samples taken from 3 vertical profiles (with 4 to 11 samples per profile) down the head scarp allow us to determine the timing of the head scarp exposure and denudation (S1 to S3) (Fig. 3a). Fig. 4 describes the exposure history considered to estimate the deglaciation (Tg) and the destabilization (Td) ages. Exposure ages were computed assuming no erosion since initiation of the landslide and with negligible chemical weathering. This assumption is supported by the: (1) short exposure duration (<20 ka) with respect to the long ^{10}Be half-life; (2) quartz-rich composition of the rock; and (3) local preservation on the scarp of mechanical striae generated by the hanging wall block downward displacement. In this context the resulting ages are maximum ages. Before the retreat of the glacier (Tg) (Fig. 4a), ^{10}Be concentration in glacially polished bedrock samples (C_{Pg}) and scarp samples (C_S) is negligible due to the shielding effect of the glacier for cosmic rays. When the last glacier melted (Tg) (Fig. 4b), exposure to cosmic rays began. The snow shielding (S_s) is only considered for horizontal surfaces (Fig. 4b and c). Reasonable assumptions were taken into account for the height ($H_S = 1$ to 2 m), the duration in months ($M_S = 4$ months), physical properties (density ($\rho_S = 0.28$) and attenuation length ($\Lambda_S = 160$ g.cm^{-2})) of snow:

$$S_S = \frac{M_S}{12} e^{\frac{-\rho_S H_S}{\Lambda_S}} + \frac{12 - M_S}{12} \tag{2}$$

For the glacially polished bedrock samples, nuclides concentration in quartz (C_{Pg}) accumulated directly at the surface between Tg and today (Fig. 4b and c) is given by:

$$C_{Pg} = \frac{P_{Pg}}{\lambda}\left(1 - e^{-\lambda Tg}\right) \tag{3}$$

where P_{Pg} is the normalized production rate of sample Pg.

For the scarp samples, the exposure history is more complex. Just before gravitational destabilization, between Tg and Td (Fig. 4b), the nuclide concentration (C_0) accumulated in quartz as a function of depth (Di) is given by:

$$C_0 = \frac{P_{S-0}}{\lambda}\left(1 - e^{-\lambda(Tg - Td)}\right)\left\{P_\eta e^{\frac{-\rho Di}{\Lambda_\eta}} + P_{\mu f} e^{\frac{-\rho Di}{\Lambda_{\mu f}}} + P_{\mu s} e^{\frac{-\rho Di}{\Lambda_{\mu s}}}\right\} \tag{4}$$

where P_η, $P_{\mu f}$ and P_{μ_s} refer to the relative contributions of neutrons, and fast and slow muons (97.85%, 0.65% and 1.5% respectively (Braucher et al., 2003)); Λ_η, $\Lambda_{\mu f}$ and Λ_{μ_s} are the effective attenuation length for neutrons, and fast and slow muons (150, 5300 and 1500 g cm^{-2} respectively (Braucher et al., 2003)); ρ is the rock density (2.5) and P_{S-0} is the normalized production rate at the top of the scarp (Fig. 4). As soon as the scarp develops (between Td and the present day), the concentration of

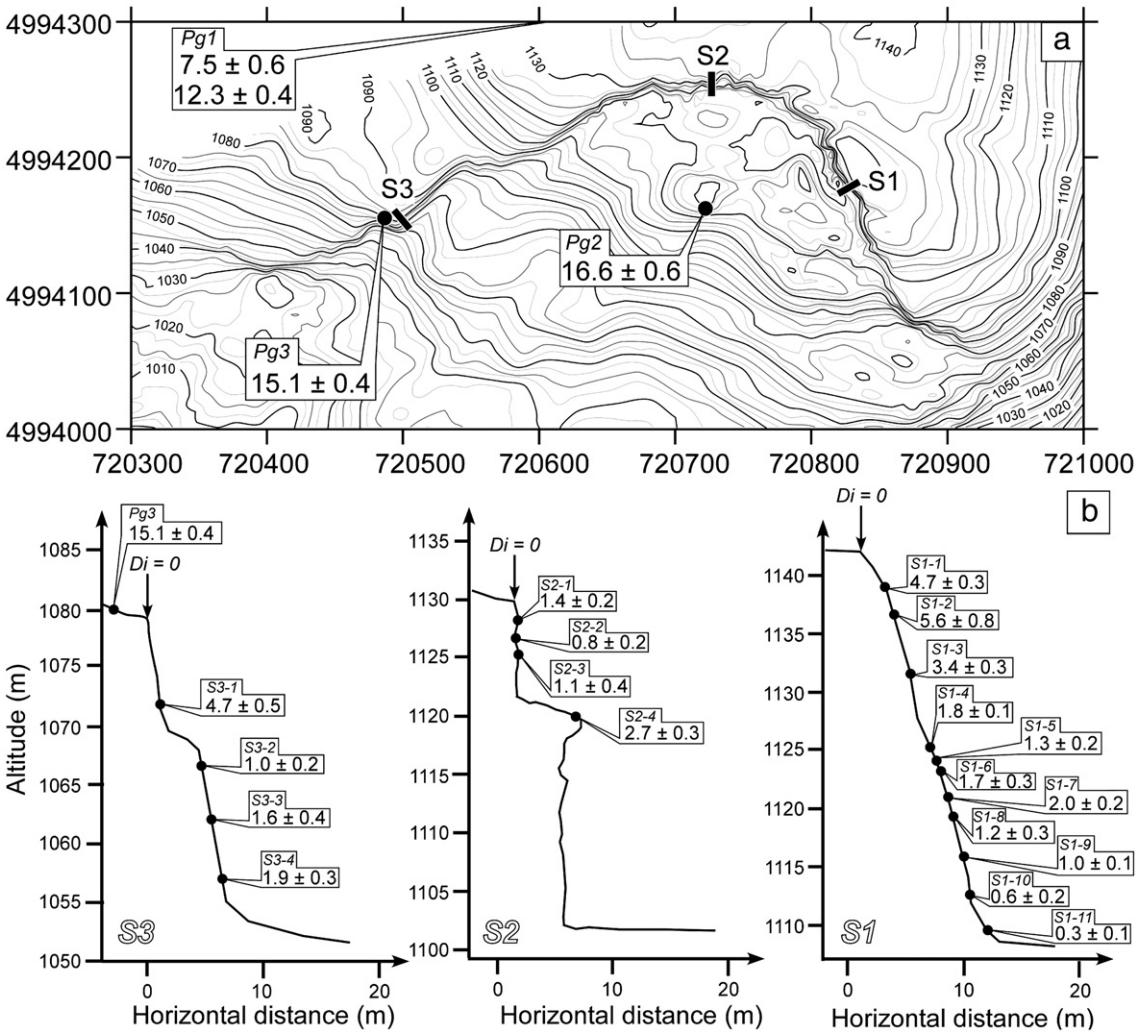

Fig. 5. (a) Topographical map of the Séchilienne head scarp area with the location and exposure ages (in ka) of analysed samples, Pg1 is located northward, out of the frame (see Fig. 3a). (b) Cross sections of sampling profiles S1, S2, S3 scale 1/1 with the location and exposure ages (in ka) of analysed samples. Di = 0: location of the top of the scarp (see Fig. 4).

nuclides in the samples of this vertical surface results from two contributions (Fig. 4c). The first is the ^{10}Be production resulting from cosmic rays penetrating the horizontal surface above the scarp. The resulting concentration (C_1) depends on half the normalized production rate at the top of the scarp (P_{S-0}) taking into account the attenuation of the cosmic rays due to the thickness Di of the rock above the sample. It is given by:

$$C_1 = \frac{1}{2}\frac{P_{S-0}}{\lambda}\left(1 - e^{-\lambda T_d}\right)\left\{P_\eta e^{\frac{-\rho Di}{\Lambda_\eta}} + P_{\mu f} e^{\frac{-\rho Di}{\Lambda_{\mu f}}} + P_{\mu s} e^{\frac{-\rho Di}{\Lambda_{\mu s}}}\right\} \quad (5)$$

The second contribution results from cosmic rays striking straight the vertical surface of the scarp. The concentration (C_2) depends on the normalized production rate on the scarp sample (P_{S-i}) and is given by:

$$C_2 = \frac{P_{S-i}}{\lambda}\left(1 - e^{-\lambda T_d}\right) \quad (6)$$

At present, the ^{10}Be concentration into the scarp samples is assumed to be:

$$C_s = C_0 + C_1 + C_2 \quad (7)$$

This equation allows determining Td using the value of Tg calculated from Eq. (3) using the concentrations measured in the glacially polished rock samples.

The resulting CRE ages are absolute ages given in ^{10}Be ka. Their uncertainties derive from two types of sources, on one hand analytical uncertainties in the ^{10}Be concentration in quartz samples (counting statistics, conservative estimate of 1% instrumental variability and uncertainty in the chemical blank) and on the other hand on a maximal 15% uncertainty on the ^{10}Be production rates.

4. Results and interpretation

4.1. Glacially polished bedrock dating

Three sites were sampled on the glacial shoulder of the Mont Sec Plateau between 1080 and 1121 m a.s.l. (Table 1), two in the stable area (Pg1 and Pg3) and one in the landslide (Pg2) (Fig. 5a). The resulting CRE ages range from 7.5 to 16.6 ^{10}Be ka. At site Pg1 located on a glacially polished surface outcropping within a peat bog, two samples five meters apart yield significantly different ages of 7.5 ± 0.6 and 12.3 ± 0.4 ^{10}Be ka (Table 1, Fig. 5a). Sample Pg3 located 2 m beside the head scarp is dated at 15.1 ± 0.4 ^{10}Be ka (Table 1, Fig. 5a and b). Pg2, sampled on the top of a bedrock block bounded by fractures and located inside the destabilized area, provides an age of 16.6 ± 0.6 ^{10}Be ka (Table 1, Fig. 5a).

In the case of surfaces shaped by glaciers, the interpretation of CRE ages is dependent on the presence of screens to cosmic rays such as moraine and/or peat bog. If no screen was deposited on the site, the

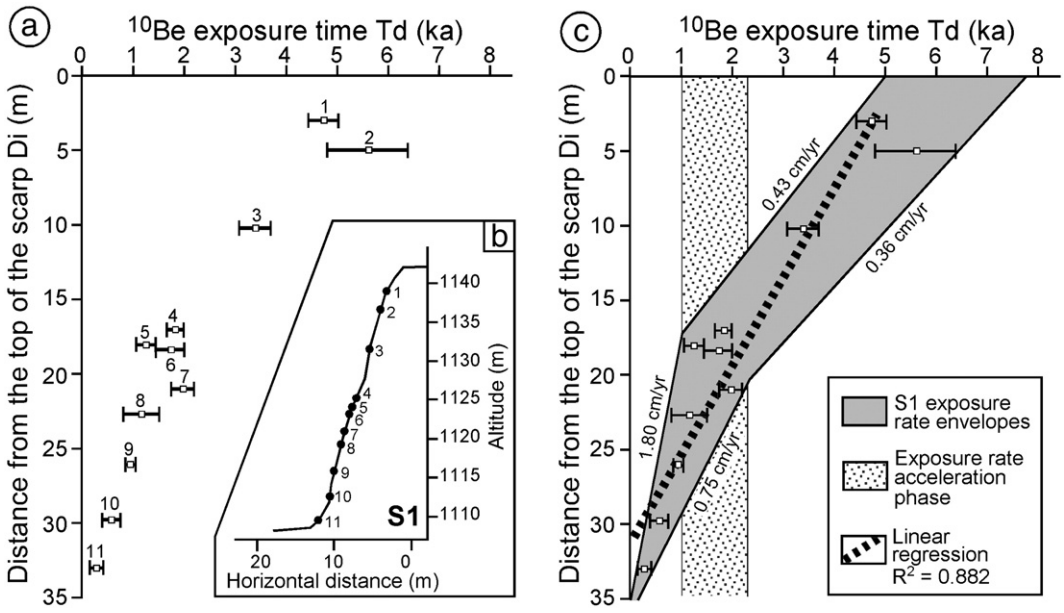

Fig. 6. (a) ^{10}Be exposure ages plotted versus Di with $\pm\sigma$ of analytical uncertainties of profile S1. (b) Cross section of sampling profile S1 on the Séchilienne head scarp. (c) The raw ^{10}Be exposure ages plotted versus Di with $\pm\sigma$ of analytical uncertainties of profile S1 are interpreted in terms of exposure rates variations.

exposure age corresponds to the ice retreat as it is assumed in our model (Fig. 4). However, if moraine deposits or peat bog were laid down, the significance of the CRE ages depends on the time these screens persisted on the bedrock. This age thus corresponds to the removal of any cover and in this case the resulting age is younger than time of ice retreat.

Given the scattered CRE ages obtained on the glacial shoulder for samples collected at similar elevations (~1100 m), we interpret the older age at Pg2 (16.6 ± 0.6 ^{10}Be ka) as the minimal age of the last retreat of the Romanche Glacier around 1100 m a.s.l. in the Séchilienne landslide area (Tg in Fig. 4). The timing of glacial retreat is consistent with the onset of the formation of the Mont Sec peat bog dated by ^{14}C at 11.5 ± 0.5 ka BP (Muller et al., 2007) in the vicinity of Pg1, in a place that was likely previously covered by moraine.

4.2. Head scarp dating

Three 30 to 35 m high vertical profiles (S1 to S3) were sampled along the landslide head scarp (see Fig. 3 for location, and Fig. 5). Eleven samples were collected along the 35 m high vertical profile S1, which exhibits a regular shape and whose foot is buried below fallen rock fragments of unknown thickness (Fig. 5b). Exposure ages Td, along with error bars, are given in Table 1 and are plotted versus vertical distance along the scarp Di in Fig. 6a. As expected, exposure age values more or less regularly decrease from the top (4.7 ^{10}Be ka, point 1 in Fig. 6a and b) to the bottom (<1.0 ^{10}Be ka) of the scarp, showing a progressive head scarp exposure resulting from the downward vertical motion of the depletion zone. These results show the downward motion of the depletion zone along the scarp is continuous with time. We fitted a regression line to the 11 experimental data, shown

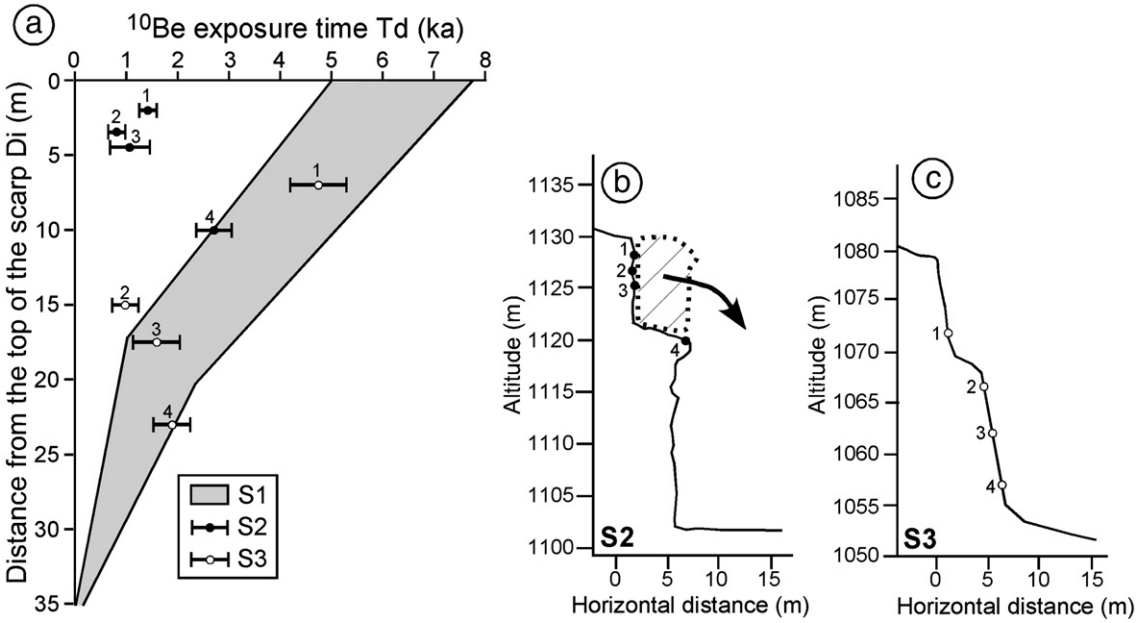

Fig. 7. (a) ^{10}Be exposure age plotted versus Di with $\pm\sigma$ of analytical uncertainties of profiles S2 and S3 with the S1 exposure rate envelopes in grey. (b) Cross section of sampling profile S2 on the head scarp with model of the recent rockfall event to explain the young ages at the top of the scarp plotted on Fig. 6a. (c) Cross section of S3 on the head scarp.

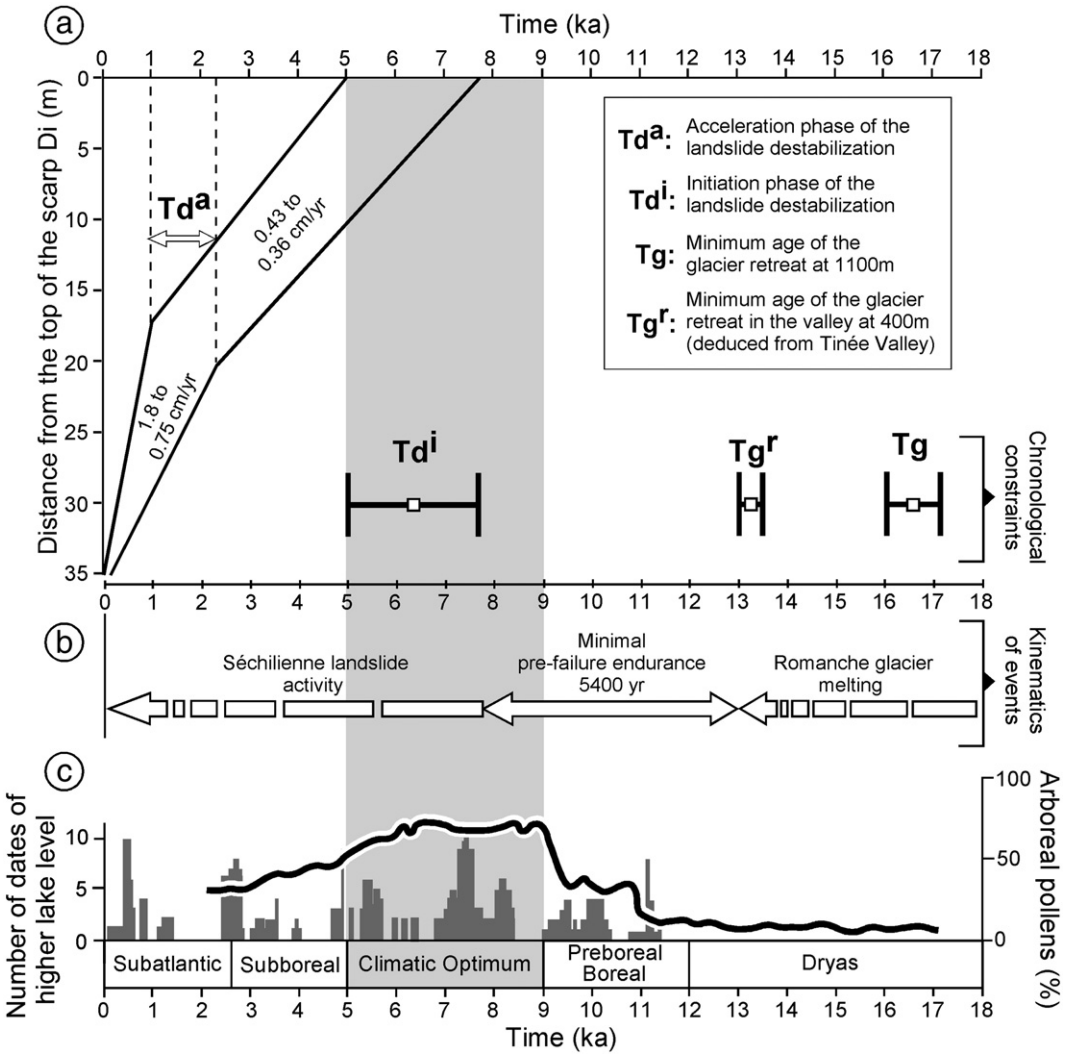

Fig. 8. (a) The ^{10}Be exposure age envelope of profile S1 plotted as a function of time provide chronological constraints (Tg, Tg^r, Td^i) and show the relationship between the initiation phase (Td^i) of the landslide and the Holocene Climatic Optimum. The acceleration phase of landslide destabilization (Td^a) and displacement rates are also indicated. (b) Kinematics of the events deduced from the chronological data related to glacier melting and landslide activity yielded a minimal pre-failure endurance. (c) Distribution of the dates of higher lake-level events reconstructed in the Jura mountains, the northern French Pre-Alps and the Swiss Plateau during the Holocene (histogram, Magny, 2004, 2007) and evolution of arboreal pollens (curve, de Beaulieu, 1977) through late Quaternary.

in Fig. 6c. Even if the linear equation with a constant scarp exposure rate of 0.6 cm/yr yields a satisfactory fit ($R^2 = 0.882$), it fails to explain the recent vertical motions. Indeed, more recent data (points 9 to 11 in Fig. 6a and b) provide a mean scarp exposure rate of about 1.08 cm/yr which is closer to measured present-day values (1.3 cm/yr). On the contrary, the linear law yields a twice lower rate. These results suggest that the scarp exposure rate increased with time since the failure initiation. If we draw the two envelope lines passing through the extreme values considering error bars (Fig. 6c), exposure scarp ages are distributed inside a narrow area (grey in Fig. 6c). The slopes of the envelopes suggest that two periods with different scarp exposure rates can be distinguished with a rate increase at mid-scarp (Di between 17 and 20 m) between 1 and 2.3 ^{10}Be ka (dotted area in Fig. 6c). The first stage of exposure is characterized by low rate values (between 0.36 and 0.43 cm/yr, Fig. 6c) while the second stage displays high rate values (between 0.75 and 1.80 cm/yr, Fig. 6c), in agreement with measured present-day values. The intersections of the envelope lines with the horizontal axis Di = 0 allow the initiation time of the landslide failure to be bracketed between 5.0 and 7.8 ^{10}Be ka.

The two other vertical profiles (S2 and S3) were located westward (Fig. 5a) of profile S1 and exhibit a topography less regular than profile S1 (Fig. 5b). Four samples were collected on each profile and the exposure ages are given in Table 1 and Fig. 7a. In this figure are also plotted the envelopes determined from profile S1. For the same vertical position on the cliff (Di), exposure ages are similar or close to those of profile S1 (Table 1, Fig. 7a, b and c) except for the three upper samples of profile S2 (1 to 3, in Fig. 7a) which gave younger ages. These latter can be explained by the presence of an intermediate shelf on profile S2 (Fig. 7b), which suggests the occurrence of a rock-fall event at the top of the scarp posterior to the scarp exposure. Since the length of the landslide head scarp comprised between profiles S1 and S3 represents 65% of its total length (Fig. 4a), the exposure ages (Td) obtained for S2 and S3 plot within the S1 envelope (Fig. 7a), suggesting that the formation of the head scarp occurred either synchronously in every point between S1 and S3 or with a very fast lateral propagation. Additionally, the similar mean rate of head scarp exposure between S1 and S3 indicate synchronous settling kinematics of the depletion zone at the bottom of the head scarp as a whole.

5. Discussion

The CRE data obtained on the Sechilienne slope show the glacial retreat at 1100 m a.s.l. occurs at 16.6 ± 0.6 ^{10}Be ka. Moreover, at the same elevation the onset of the Séchilienne head scarp is dated 6.4 ± 1.4 ^{10}Be ka. This implies a minimal time

span of 8200 yr between the two events at 1100 m a.s.l., taking into account the error bars (Fig. 8a). However, these data restricted to the 1100 m elevation are not sufficient to understand the relationships between the glacier melting kinematics and the initiation of the whole slope instability. Temporal constraints are therefore needed to estimate the time span between the total downwastage of the ice and the initiation of the resulting instability. This duration expresses the slope response to progressive stress release following slope debutressing. In the case of the Romanche Valley age data about the total downwastage of the glacier are not available.

We propose to transpose to the Romanche Valley, data available from another large alpine glacial valley, the Tinée Valley. Indeed, according to Vincent et al. (2004), temperature variations recorded over the last century at the scale of the Alpine Arc generate similar ice ablation dynamics for glaciers located several hundreds kilometres apart. The Tinée valley is located 130 km southeast from the Romanche Valley, in a similar geological setting (External Crystalline Massif of Argentera), and displays a similar geometry with a 1000 m height between the bottom of the valley and the glacial shoulder. This valley provides chronological constraints on its total downwastage. The bottom of the valley (1100 m a.s.l.) dates to 13.3 ± 0.1 ka BP (Bigot-Cormier et al., 2005) by ^{14}C age on travertine. At 13.3 ka BP the bottom of the Romanche Valley at 400 m a.s.l. was probably already ice-free. This estimation is consistent with ^{10}Be dates on glacial retreat ranging from 7 to 12 ka (Cossart et al., 2008) obtained in the neighbouring valleys (External Crystalline Massif of Pelvoux) for elevations above 2000 m a.s.l. These chronological constraints suggest that for the Romanche Valley, between the 16.6 ± 0.6 ^{10}Be ka exposure age of Pg2 glacially polished surface at 1100 m a.s.l. and the 13.3 ± 0.1 ka BP downwastage at 400 m a.s.l., 750 m of ice melted in 3300 yr (Figs. 7b and 8a). In this case, the minimum time interval between the total downwastage of the Romanche Valley ice and the initiation of failure along the Séchilienne head scarp is therefore 5400 yr (Fig. 8b). This duration can be considered as a pre-failure endurance (Ballantyne, 2002), i.e. the time interval following total melting of ice in the valley during which the slope endures the new state of stress before the initiation of failure. This duration therefore reveals the dynamic adjustment of the rocky slopes resulting from the interaction between debutressing (stress variation stemming from glacial unloading) and the strength of the rock massif. The mechanical behaviour of the slope is controlled by internal factors including lithology, joint network density and orientation and external ones such as seismic events, climatic changes and anthropic activity. For the Séchilienne landslide the 5400 yr value is compatible with the 5700 yr average of pre-failure endurance obtained by Cruden and Hu (1993) from a negative exhaustion model and with the 7000 yr limit value deduced from the study of Scottish rock-slope failures (Ballantyne, 2002).

At the scale of the Alpine Arc, the recent CRE studies of major landslides show that the initiation of instability does not immediately follow deglaciation but occurs several thousand years after the valley is totally ice-free. The estimated pre-failure endurance is thus more than 3000 yr for la Clapière landslide (French Western Alps, Bigot-Cormier et al., 2005), more than 2500 yr for the Flims rockslide (Swiss Central Alps, Ivy-Ochs et al. 2009), more than 4000 yr for the Val Viola rockslide (Italian Central Alps, Hormes et al., 2008), and more than 2000 yr for the Fernpass rockslide (Austrian Eastern Alps, Prager et al., 2009). Considering data available for major alpine landslides, Ivy-Ochs et al. (2009) suggest slope failure did not occur during deglaciation but during mid-Holocene time when climate became markedly warmer and wetter. In the case of the Séchilienne landslide, the CRE data show that the initiation stage occurred during the Holocene Climatic Optimum, an event ranging from 9.0 to 5.0 ka BP (grey on Fig. 8) In the case of the La Clapière landslide, the initiation stage also occurred during the Climatic Optimum. In the western Alps, this period is characterized by an increase of the mean temperature of 1 to 2° (Davis et al., 2003), an increase of the density of forest cover (de Beaulieu, 1977) and an increase in lake level due to heavy annual precipitation (Magny, 2004, 2007) (Fig. 8c). The combination of these different climatic characteristics indicates that the Climatic Optimum was a warmer and wetter period. The exposure rates (Fig. 8a) obtained from the Séchilienne head scarp show that the activity of the landslide is continuous from its triggering until present day, with an acceleration phase between 2.3 and 1.0 ka, which coincides with the subatlantic chronozone. (Fig. 8a and c). This warmer and wetter phase allows displacement rates to reach 0.75 to 1.80 cm/yr (Figs. 6 and 8a). We suggest that slide acceleration is due to the decrease of mechanical properties within the rock mass or along slip surfaces, resulting from progressive slope motion. These high displacement rates are similar to those recorded during the last twenty years by instrumental survey (0.7 to 1.6 cm/yr; Vengeon et al., 1999). Monitoring data suggest a correlation between the increase of displacement rate of the whole slope with heavy rainfall thus clearly pointing out the major role of precipitation in slope instability. Therefore, an external hydrological parameter seems to have a worsening effect, adding to the decrease of the mechanical properties of the rock mass to trigger and maintain the Séchilienne landslide dynamics. Nevertheless the mechanical properties of a massif can also be weakened by seismic events. In fact the Séchilienne landslide is located in a zone (Romanche Valley, Belledonne Massif) affected by recurring seismicity. The potential maximal magnitude estimated from the instrumental seismicity is lower than $M_L = 3.5$ (Thouvenot et al., 2003). It cannot be excluded that seismic activity played a role in the Séchilienne landslide movement but this link is not demonstrated at the present time.

6. Conclusions

CRE data acquired from vertical sampling profiles along the Séchilienne head scarp provide chronological constraints on the failure time of this major alpine landslide. Exposure ages at 1100 m a.s.l. in the head scarp area indicate that the glacier retreated at 16.6 ± 0.6 ^{10}Be ka and that the head scarp of the landslide was triggered at 6.4 ± 1.4 ^{10}Be ka. Comparing the date of the rock-slope failure initiation to the estimated age of total downwastage of the valley yields a minimal pre-failure endurance of 5400 yr. Therefore slope destabilization does not appear as an immediate consequence of debutressing in the Romanche Valley. This result is consistent with those obtained for other large alpine landslides (Flims, Val Viola, Fernpass, La Clapière). The initiation phase of the Séchilienne landslide occurred during the Holocene Climatic Optimum, a warmer and wetter interval. This result suggests that temperature and precipitation changes at that period had a significant – triggering or worsening – effect on the Séchilienne failure in the glacial Romanche Valley. High spatial resolution CRE data (3 m spacing) collected on vertical profiles provides an innovative contribution to understanding the Séchilienne landslide kinematics during the Holocene. Results show the head scarp exposure to be progressive – and then the sliding process to be continuous – from failure initiation to present with a mean rate of about 0.6 cm/yr. Exposure age distribution, however, suggest an increase of the exposure rate between 2.3 and 1 ka up to 1.08 cm/yr, mean value. After this acceleration phase, the exposure rates are similar to those obtained by present day monitoring (1.3 cm/yr).

Acknowledgments

We thank the two anonymous reviewers for thorough critical reviews. This work was supported by the ANR ANCEMT. We thank M.Arnold and G.Aumaître for their valuable assistance during the ^{10}Be measurements performed at the ASTER AMS national facility (CEREGE, Aix en Provence) which is supported by the INSU/CNRS, the French Ministry of Research and Higher Education, IRD and CEA.

We gratefully acknowledge M. Gidon for utilizing the photograph of the Séchilienne landslide.

References

Alfonsi, P., 1997. Relation entre les paramètres hydrogéologiques et la vitesse dans les glissements de terrain. Exemples de La Clapière et de Séchilienne (France). Rev. Fr. Geotech. 79, 3–12.

Augustinus, P.C., 1995. Rock mass strength and stability of some glacial valley slopes. Zeitsschrift Geomorphol. 39, 55–68.

Ballantyne, C.K., 2002. Paraglacial geomorphology. Quat. Sci. Rev. 21, 1935–2017.

Ballantyne, C.K., Stone, J.O., 2004. The Beinn Alligin rock avalanche, NW Scotland: cosmogenic Be-10 dating, interpretation and significance. Holocene 14, 461–466.

Barféty, J.C., Gidon, M., Montjuven, t.G., 1970. Extension et importance des glissements superficiels aux abords méridionaux de Grenoble. Geol. Alp. 46, 17–22.

Bigot-Cormier, F., Braucher, R., Bourlès, D., Guglielmi, Y., Dubar, M., Stéphan, J.F., 2005. Chronological constraints on processes leading to large active landslides. Earth Planet. Sci. Lett. 235, 141–150.

Blair, R.W., 1994. Moraine and valley wall collapse due to rapid deglaciation in Mount Cook National Park, New Zealand. Mountain Res. Dev. 14, 347–358.

Braucher, R., Brown, E.T., Bourlès, D., Colin, F., 2003. In situ-produced ^{10}Be measurements at great depths: implications for production rates by fast muons. Earth Planet. Sci. Lett. 211, 251–258.

Brown, E.T., Edmond, J.M., Raisbeck, G.M., Yiou, F., Kurz, M.D., Brook, E.J., 1991. Examination of surface exposure ages of moraines in Arena Valley, Antartica, using in situ produced ^{10}Be and ^{26}Al. Geochim. Cosmochim. Acta 55, 2269–2283.

Brown, E.T., Bourlès, D., Burchfield, B., Deng, Q., Li, J., Molnar, P., Raisbeck, G.M., Yiou, F., 1998. Estimation of slip rates in the southern Then Shan using cosmic ray exposure dates of abandoned alluvial fans. Geol. Soc. Am. Bull. 110, 377–386.

Carlson, A.E., Clark, P.U., Raisbeck, G.M., Brook, E.J., 2007. Rapid Holocene deglaciation of the Labrador sector of the Laurentide Ice Sheet. J. Climate 20, 5126–5133.

Cossart, E., Braucher, R., Fort, M., Bourlès, D.L., Carcaillet, J., 2008. Slope instability in relation to glacial debutressing in alpine areas (upper durance catchment, southeastern France): Evidence from field data and ^{10}Be cosmic ray exposure ages. Geomorpholgy 95, 3–26.

Cruden, D.M., Hu, X.Q., 1993. Exhaustion and steady states models for predicting landslides hazards in the Canadian Rocky Mountains. Geomorpholgy 8, 279–285.

Davis, B.A.S., Brewer, S., Stevenson, A.C., Guiot, J., 2003. The temperature of Europe during the Holocene reconstructed from pollen data. Quat. Sci. Rev. 22, 1701–1716.

de Beaulieu, J.L., 1977. Contribution pollenanalytique à l'histoire tardiglaciaire et holocène de la végétation des Alpes méridionales françaises. PhD thesis, Université Aix-Marseille III, Marseille, 391 pp.

Delmas, M., Gunnell, Y., Braucher, R., Calvet, M., Bourlès, D., 2008. Exposure age chronology of the last glaciation in the eastern Pyrenees. Quat. Res. 69, 231–241.

Deplazes, G., Anselmetti, F.S., Hajdas, I., 2007. Lake sediments deposited on the Flims rockslide mass: the key to date the largest mass movement of the Alps. Terra Nova 19, 252–258.

Dunne, A., Elmore, D., Muzicar, P., 1999. Scaling of cosmogenic nucleide production rates for geometric shielding and attenuation at depth on sloped surfaces. Geomorphology 27, 3–11.

Duranthon, J.P., Effendiantz, L., Memier, M., Previtali, I., 2003. Apport des méthodes topographiques et topométriques au suivi du versant rocheux instable des ruines de Séchilienne. Revue XYZ 94, 31–38.

Durville, J.L., Effendiantz, L., Pothérat, P., Marchesini, P., 2004. The Séchilienne landslide. In: Bonnard, C., Forlati, F., Scavia, C. (Eds.), Identification and mitigation of large landslide risks in Europe. A.A. Balkema, Rotterdam, The Netherlands, pp. 253–269.

Erismann, T.H., Abele, G., 2001. Dynamics of Rockslides and Rockfalls. Springer-Verlag, Berlin. 316 pp.

Evans, S.G., Clague, J.J., 1994. Recent climatic change and catastrophic geomorphic processes in. mountain environments. Geomorphology 10, 107–128.

Evrard, H., Gouin, T., Benoit, A., Duranthon, J.P., 1990. Séchilienne, risques majeurs d'éboulements en masse; point sur la surveillance du site. Bull. de Liaison des Ponts et Chaussées 165, 7–16.

Gardner, J.S., 1980. Frequency, magnitude, and spatial distribution in the Highwood Pass area, Alberta, Canada. In: Coates, D.R., Vitek, J.D. (Eds.), Thresholds in Geomorphology. Allen and Unwin, Boston, pp. 171–192.

Giraud, A., Rochet, L., Antoine, P., 1990. Processes of slope failure in cristallophyllian formations. Eng. Geol. 29, 241–253.

Gosse, J.C., Phillips, F.M., 2001. Terrestrial in situ cosmogenic nucleides: theory and application. Quat. Sci. Rev. 20, 1475–1560.

Gosse, J.C., Klein, J., Evenson, E.B., Lawn, B., Middleton, R., 1995. Beryllium-10 dating of the duration and retreat of the last Pinedale glacial sequence. Science 268, 1329–1333.

Guglielmi, Y., Vengeon, J.M., Bertrand, C., Mudry, J., Follacci, J.P., Giraud, A., 2002. Hydrogeochemistry: an investigation tool to evaluate infiltration into large moving rock masses (case study of La Clapière and Séchilienne alpine landslides). Bull. Eng. Geol. Environ. 61, 311–324.

Hippolyte, J.C., Brocard, G., Tardy, M., Nicoud, G., Bourlès, D., Braucher, R., Ménard, G., Souffaché, B., 2006. The recent fault scarps of the Western Alps (France): Tectonic surface ruptures or gravitational sacking scarps? A combined mapping, geomorphic, levelling, and ^{10}Be dating approach. Tectonophysics 418, 255–276.

Holm, K., Bovis, M.J., Jakob, M., 2004. The landslide response of alpine basins to post-Little Ice Age glacial thinning and retreat in southwestern British Columbia. Geomorphology 57, 201–216.

Hormes, A., Ivy-Ochs, S., Kubik, P.W., Ferreli, L., Michetti, A.M., 2008. ^{10}Be exposure ages of rock avalanche and a late glacial moraine in Alta Valtellina, Italian Alps. Quat. Int. 190, 136–145.

Ivy-Ochs, S., Poschinger, A.V., Synal, H.A., Maisch, M., 2009. Surface exposure dating of the Flims landslide, Graubünden, Switzerland. Geomorphology 103, 104–112.

Korup, O., 2008. Rock type leaves topographic signature in landslide-dominated mountain ranges. Geophys. Res. Lett. 35, L11402. doi:10.1029/2008GL034157.

Korup, O., Clague, J.J., Hermanns, R.L., Hewitt, K., Strom, A.L., Weidinger, J.T., 2007. Giant landslides, topography, and erosion. Earth Planet. Sci. Lett. 261, 578–589.

Le Roux, O., Schwartz, S., Gamond, J.F., Jongmans, D., Tricart, P., Sebrier, M., 2008. Interaction between tectonic and erosion processes on the morphogenesis of an alpine valley: geological and geophysical investigations in the lower Romanche valley (Belledonne massif, western Alps). Int. J. Earth Sci. (Geol Rundsch). doi:10.1007/s00531-008-0393-1.

Magny, M., 2004. Holocene climate variability as reflected by mid-European lake-level fluctuations and its probable impact on prehistoric human settlements. Quat. Int. 113 (1), 65–79.

Magny, M., 2007. Climate oscillations and hydrological variations in Europe over the last 15,000 years. Lettre pigb-pmrc-France 20, 72–76.

Meric, O., Garambois, S., Jongmans, D., Wathelet, M., Chatelain, J.L., Vengeon, J.M., 2005. Application of geophysical methods for the investigation of the large gravitational mass movement of Séchilienne, France. Can. Geotech. J. 42, 1105–1115.

Montjuvent, G., Winistorfer, J., 1980. Glaciations quaternaires dans les Alpes franco-suisses et leur piedmont. Geol. Alp. 56, 251–282.

Muller, S.D., Nakagawa, T., de Beaulieu, J.L., Court-Picon, M., Carcaillet, C., Miramont, C., Roiron, P., Boutterin, C., Ali, A.A., Bruneton, H., 2007. Postglacial migration of silver fir (Abies alba Mill.) in the southwestern Alps. J. Biogeography 34, 876–899.

Nishiizumi, K., Imamura, M., Caffee, M.W., Southon, J.R., Finkel, R.C., McAninch, J., 2007. Absolute calibration of ^{10}Be standards. Nucl. Instrum. Methods Phys. Res., B 258, 403–413.

Owen, L.A., Gualtieri, L., Finkel, R.C., Caffee, M.W., Benn, D.I., Sharma, M.C., 2001. Cosmogenic radionuclide dating of glacial landforms in the Lahul Himalaya: defining the timing of Late Quaternary glaciation. J. Quat. Sci. 16 (6), 555–563.

Pothérat, P., Alfonsi, P., 2001. Les mouvements de versant de Séchilienne (Isère). Prise en compte de l'héritage structural pour leur simulation numérique. Revue Française de Géotechnique 95–96, 117–131.

Prager, C., Ivy-Ochs, S., Ostermann, M., Synal, H.A., Patzelt, G., 2009. Geology and radiometric 14C-, 36Cl- and Th-/U-dating of the Fernpass rockslide (Tyrol, Austria). Geomorphology 103, 93–103.

Rochet, L., Giraud, A., Antoine, P., Evrard, H., 1994. La déformation du versant Sud du Mont sec dans le secteur des ruines de Séchilienne (Isère, France). Bull. Int. Assoc. Eng. Geol. 50, 75–87.

Seijmonsbergen, A.C., Woning, M.P., Verhoef, P.N.W., de Graaff, L.W.S., 2005. The failure mechanism of a Late Glacial Sturzstrom in the Subalpine Molasse (Leckner Valley, Vorarlberg, Austria). Geomorphology 66, 277–286.

Siame, L., Braucher, R., Bourlès, D., 2000. Les nucléides cosmogéniques produits in-situ: de nouveaux outils en géomorphologie quantitative. Bull. Soc. Geol. Fr. 171, 383–396.

Stone, J.O., 2000. Air pressure and cosmogenic isotope production. J. Geophys. Res. 105, 23753–23759.

Thouvenot, F., Frechet, J., Jenatton, L., Gamond, J.F., 2003. The Belledonne Border Fault: identification of an active seismic strike-slip fault in the western Alps. Geophys. J. Int. 155, 174–192.

Vengeon, J.M., 1998. Deformation et rupture des versants en terrain métamorphique anisotrope. Apport de l'étude des ruines de Séchilienne. PhD thesis, Université Grenoble I, Grenoble, 186 pp.

Vengeon, J.M., Giraud, A., Antoine, P., Rochet, L., 1999. Analysis of the deformation and toppling of rock slopes in crystallophyllian terrain. Can. Geotech. J. 36, 1123–1136.

Vincent, C., Kappenberger, G., Valla, F., Bauder, A., Funk, M., Le Meur, E., 2004. Ice ablation as evidence of climate change in the Alps over the 20th century. J. Geophys. Res. 109, D10104. doi:10.1029/2003JD003857.